SANDIA REPORT
SAND2000-8230
Unlimited Release
Printed March 2000

Band Spreading in Two-Dimensional Microchannel Turns for Electrophoretic or Electroosmotic Species Transport

S. K. Griffiths, R. H. Nilson

Prepared by
Sandia National Laboratories
Albuquerque, New Mexico 87185 and Livermore, California 94550

Sandia is a multiprogram laboratory operated by Sandia Corporation, a Lockheed Martin Company, for the United States Department of Energy under Contract DE-AC04-94AL85000.

Approved for public release; further dissemination unlimited.

Sandia National Laboratories

Issued by Sandia National Laboratories, operated for the United States Department of Energy by Sandia Corporation.

NOTICE: This report was prepared as an account of work sponsored by an agency of the United States Government. Neither the United States Government, nor any agency thereof, nor any of their employees, nor any of their contractors, subcontractors, or their employees, make any warranty, express or implied, or assume any legal liability or responsibility for the accuracy, completeness, or usefulness of any information, apparatus, product, or process disclosed, or represent that its use would not infringe privately owned rights. Reference herein to any specific commercial product, process, or service by trade name, trademark, manufacturer, or otherwise, does not necessarily constitute or imply its endorsement, recommendation, or favoring by the United States Government, any agency thereof, or any of their contractors or subcontractors. The views and opinions expressed herein do not necessarily state or reflect those of the United States Government, any agency thereof, or any of their contractors.

Printed in the United States of America. This report has been reproduced directly from the best available copy.

Available to DOE and DOE contractors from
Office of Scientific and Technical Information
P.O. Box 62
Oak Ridge, TN 37831

Prices available from (703) 605-6000
Web site: http://www.ntis.gov/ordering.htm

Available to the public from
National Technical Information Service
U.S. Department of Commerce
5285 Port Royal Rd
Springfield, VA 22161

NTIS price codes
Printed copy: A03
Microfiche copy: A01

SAND2000-8230
Unlimited Release
Printed March 2000

Band Spreading in Two-Dimensional Microchannel Turns for Electrophoretic or Electroosmotic Species Transport

Stewart K. Griffiths and Robert H. Nilson
Sandia National Laboratories
Livermore, California 94551-0969

ABSTRACT

Analytical and numerical methods are employed to investigate species transport by electrophoretic or electroosmotic motion in the curved geometry of a two-dimensional turn. Closed-form analytical solutions describing the turn-induced diffusive and dispersive spreading of a species band are presented for both the low and high Peclet number limits. We find that the spreading due to dispersion is proportional to the product of the turn included angle and the Peclet number at low Peclet numbers. It is proportional to the square of the included angle and independent of the Peclet number when the Peclet number is large. A composite solution applicable to all Peclet numbers is constructed from these limiting behaviors. Numerical solutions for species transport in a turn are also presented over a wide range of the included angle and the mean turn radius. Based on comparisons between the analytical and numerical results, we find that the analytical solutions provide very good estimates of both dispersive and diffusive spreading provided that the mean turn radius exceeds the channel width. These new solutions also agree well with data from a previous study. Optimum conditions minimizing total spreading in a turn are presented and discussed.

INTRODUCTION

Microchannel systems, first explored only about ten years ago [1-5], are now under development for a wide range of applications in the detection, analysis and synthesis of chemical and biological species [6-16]. Employing channel widths from a few microns to about one millimeter, such systems may permit the broad integration and miniaturization of many processes now performed at the laboratory scale.

Many microchannel devices employ some combination of electrophoresis and electroosmotic flow on a single substrate. Electrophoresis in a stationary or fluid phase is typically used for analysis, while electroosmotic flow is employed for sample preparation and injection into the separation column [1-11,14-17]. In a few instances, electroosmotic flow is used in conjunction with electrophoresis with the intent to improve separation efficiency [18,19]. Electroosmotic flows are also used for analysis via electrochromatography in either open or packed channels [12,20-24].

Both electrophoresis and electroosmotic flow permit long-range species transport with little dispersion due to nonuniform speeds [25-27]. However, while this is true for straight channel segments, microchannel turns can produce dramatic skewing of an otherwise flat species band due to the locally nonuniform electric field or fluid velocity. Such skewing is generally irreversible because transverse diffusion redistributes species concentrations across the channel, and the net effect on the band is a large and permanent spreading of the species distribution along the channel downstream of the turn. Compositional interfaces are similarly deformed and spread by transport through a turn. As a result, elbows, wyes, tees and other common fittings are often avoided in microchannel systems. This limitation constrains system design and precludes compact channel layout on a small chip area.

Turns are a significant source of dispersion in both separation processes and routine species transport. This has been recognized for some time. In 1960 Giddings analyzed the excess band spreading induced by capillary coiling in packed-column gas-phase chromatography [28]. His analysis was based

on assumptions that the turn radius is large compared to the capillary diameter and that transverse variations of the species concentration are very small. This latter approximation is roughly equivalent to an assumption that the Peclet number is small. Under these restrictions, Giddings obtained a closed-form expression for the effective diffusivity during transport through a turn as a function of the mean speed, capillary diameter and turn radius.

In 1995 Kasicka et al. analyzed the effects of capillary coiling on capillary zone electrophoresis [29]. This study focused on cases in which transverse diffusion is negligible, corresponding to the limit of an infinite Peclet number. For such cases the authors obtained closed-form expressions describing the increased variance of the species distribution induced by a turn. Their analysis also employed the assumption of a large turn radius.

Most recently, Culbertson et al. investigated several sources of dispersion in microchannel devices [30]. As part of this study, they collected a large set of data on the increased variance of a species band downstream of a turn. These quantitative results span a very wide range of conditions and turn geometries. They also developed a physically-motivated expression describing the increased variance over all Peclet numbers. Two empirical constants appearing in this expression were obtained from a fit to their data.

Here we derive rigorous analytical solutions describing the increased band variance induced by a two-dimensional turn for either electrophoretic or electroosmotic species motion. Based on the assumption of a large turn radius, solutions are first obtained in the limits of low and high Peclet numbers. These limiting results are then combined to provide simple closed-form expressions describing both the dispersive and total spreading at all Peclet numbers. In addition, the governing equations describing the electric potential and advective and diffusive species motion are solved numerically. No approximations regarding the turn geometry are employed in this numerical approach. The analytical solutions are compared with these numerical results and with data from the previous study [30] by Culbertson et al.

GOVERNING EQUATIONS

Consider the electroosmotic flow and species transport in the curved channel of a two-dimensional turn of constant radius. The channel width is presumed constant, the top and bottom surfaces are planar, and all surfaces bounding the channel are impermeable and non-conducting. Assuming that the fluid is incompressible and that transport properties are constant, the time-dependent concentration field is governed by

$$\frac{\partial c}{\partial t} + \mathbf{u}\cdot\nabla c = D\nabla^2 c \tag{1}$$

where c is the local species concentration, t is time, $\mathbf{u} = u\mathbf{i} + v\mathbf{j}$ is the local fluid velocity, and D is the coefficient of diffusion. Further assuming that the flow is steady, that there are no applied pressure gradients and that inertial effects are small, the momentum equation may be written as

$$\mu\nabla^2\mathbf{u} = \rho_e\nabla\phi \tag{2}$$

where μ is the fluid viscosity, ρ_e is the net local charge density, and ϕ is the electric potential. Finally, for a dielectric constant, ϵ, that does not vary with position, the Poisson equation governing the electric potential is

$$\epsilon\,\nabla^2\phi = -\rho_e \tag{3}$$

The charge density, ρ_e, for equivalent ions may be related to the electric potential through the Boltzmann distribution.

In many cases of practical interest, the local fluid velocity in electroosmotic flow is proportional to the applied electric field [31]. The main conditions necessary for such similitude are a quasi-steady electric field, uniform fluid density, and uniform viscosity of the neutral fluid outside the Debye layer. Further, the Debye layer thickness must be small compared to any channel dimension, and all solid surfaces bounding the fluid must be electrically non-conducting relative to the fluid and have a uniform surface charge or surface potential. All of these conditions are usually met in microchannel systems, at least over the scale of a single turn.

Under these restrictions, the electric potential outside the Debye layer is governed by the Laplace equation

$$\nabla^2\phi = 0 \tag{4}$$

and the local fluid velocity is everywhere given by

$$\mathbf{u} = -\frac{\epsilon\zeta}{\mu}\nabla\phi \tag{5}$$

The Navier-Stokes equations presented in Eq. (2) thus need not be solved under the conditions outlined above. Moreover, when these conditions are satisfied, the electric potential and fluid velocity in any

two-dimensional channel bounded by parallel planes is strictly two-dimensional and is independent of the channel depth [31].

The equations above were developed in the context of neutral species transport in electroosmotic flow. However, when the electroosmotic fluid velocity is proportional to the electric field, these governing equations are almost the same as those describing the transport of a single charged species in electrophoretic motion in a stationary phase. That is, in both cases the species flux varies linearly with both the concentration gradient and the electric field. For electroosmotic flow, the local species flux is $\mathbf{J} = D\nabla c - \epsilon\zeta/\mu\nabla\phi$; the electrophoretic flux is $\mathbf{J} = D\nabla c + \nu z F \nabla\phi$. As such, solutions to the problem of electroosmotic flow also apply to that of electrophoresis provided that both problems are properly normalized. Further, similar equations also govern species transport in some pressure-driven flows. In both porous materials and open channels having a very small aspect ratio, the local velocity of an incompressible fluid is proportional to the pressure gradient at low Reynolds numbers, and the pressure field is governed by the Laplace equation [32,33]. The solutions presented here thus also apply to pressure-driven flows in these special cases.

To solve generally for the species concentration, we now introduce a set of dimensionless variables. The new normalized dependent variables are taken as $c^* = c/c_o$, $\mathbf{u}^* = \mathbf{u}/U$ and $\phi^* = \phi/aE$, where c_o is some reference concentration yet to be specified, E is the magnitude of the applied axial electric field far from the turn, and $U = \epsilon\zeta E/\mu$ is the Helmholtz-Smoluchowski speed for electroosmotic flow past a planar surface. We take $U = -\nu z F E$ for electrophoretic motion. The new independent variables are $y^* = (r - r_i)/a$, $s^* = (\theta - \omega t)\bar{r}/a$ and $t^* = Dt/a^2$, where r and θ are the radial and angular coordinates, r_i is the inner radius of the turn, and a is the channel width. This normalization leads to two new parameters, the Peclet number, $Pe = Ua/D$ indicating the relative magnitudes of advective and diffusive transport rates, and the inverse of the normalized radius of the turn, $\delta = a/\bar{r}$, where $\bar{r} = (r_i + r_o)/2$. Finally, we take $\omega = U/\bar{r}$ such that the transformed coordinate system rotates at a speed consistent with species motion along the turn.

Introducing these normalized variables into the primitive governing equations and rearranging slightly yields

$$\frac{1}{r^*}\frac{\partial}{\partial y^*}\left(r^*\frac{\partial\phi^*}{\partial y^*}\right) + \frac{1}{r^{*2}}\frac{\partial^2\phi^*}{\partial s^{*2}} = 0 \tag{6}$$

for Eq. (4) and

$$\mathbf{u}^* = -\left(\frac{\partial\phi^*}{\partial y^*} + \frac{1}{r^*}\frac{\partial\phi^*}{\partial s^*}\right) \tag{7}$$

for Eq. (5). The new independent variable, r^*, is introduced here merely as a convenience. It is given by

$$r^* = \frac{r}{\bar{r}} = 1 - \frac{\delta}{2}\big(1 - 2y^*\big) \tag{8}$$

where, again, $\delta = a/\bar{r}$. Boundary conditions for the normalized potential are $\partial\phi^*/\partial y^* = 0$ at $y^* = 0$ and $y^* = 1$ and $\partial\phi^*/\partial s^* = -1$ in the straight sections ahead of and behind the turn.

Given Eq. (6) and the prescribed boundary conditions, the electric potential possesses nontrivial solutions satisfying $\partial\phi^*/\partial y^* = 0$ and $\partial\phi^*/\partial s^* = -1$ everywhere in the channel when the mean radius of the turn is large compared to the channel width. The normalized fluid velocity thus possesses no radial component, and the speed along the curved channel is

$$u^* = \frac{1}{r^*} \approx 1 + \frac{\delta}{2}\big(1 - 2y^*\big) \tag{9}$$

The electroosmotic or electrophoretic speed is thus largest along the inner radius of the turn and falls about linearly with distance across the channel when the radius of the turn is large. The magnitude of the variation between the inner and outer radii is $\Delta u^* = \delta$.

Similarly introducing the normalized variables into the primitive equation governing the concentration field gives

$$\frac{\partial c^*}{\partial t^*} + Pe\left(\frac{u^*}{r^*} - 1\right)\frac{\partial c^*}{\partial s^*} = \frac{1}{r^*}\frac{\partial}{\partial y^*}\left(r^*\frac{\partial c^*}{\partial y^*}\right) + \frac{1}{r^{*2}}\frac{\partial^2 c^*}{\partial s^{*2}} \tag{10}$$

Now expanding Eq. (10) in terms of δ, and neglecting all higher-order terms, the governing equation for species motion may be rewritten as

$$\frac{\partial c^*}{\partial t^*} + Pe\big(u' - 1\big)\frac{\partial c^*}{\partial s^*} = \frac{\partial^2 c^*}{\partial y^{*2}} + \frac{\partial^2 c^*}{\partial s^{*2}} \tag{11}$$

where the apparent speed u' is given by

$$u' = \frac{u^*}{r^*} \approx 1 + \delta\big(1 - 2y^*\big) \tag{12}$$

Note that the variation in u' across the channel is twice that of u^*. This is because the apparent speed accounts for the variation in path length across the channel, as well as the actual variation in the speed.

Also note that Eq. (11) is exactly the equation describing species transport in a straight rectangular channel, except that the actual fluid speed u^* is replaced by the apparent value u'.

LOW PECLET NUMBER SOLUTION

In the limit of a low Peclet number or a large turn radius, the time required for a species band to traverse a turn is long compared to the characteristic diffusion time based on the channel width. Since the transit time is $t = \bar{r}\theta/U$, this may be expressed in terms of the normalized time as

$$t^* = \frac{Dt}{a^2} = \frac{\theta}{\delta Pe} \gg 1 \tag{13}$$

Thus t^* is large whenever the product δPe is much smaller than the included angle, θ. Late-time approximations are then appropriate when solving the governing transport equations.

Late-time solutions to Eq. (11) are well known [34-37]. As a species band is convected in a nonuniform flow field, streamwise advection and diffusion tend to spread the profile in the direction of motion. At the same time, transverse diffusion tends to reduce transverse concentration variations induced by the nonuniform velocity profile. At sufficiently late times, convective transport in the streamwise direction is just balanced by diffusive transport in the transverse direction, giving rise to the phenomenon of dispersion. This dispersion produces a mean concentration profile consistent with diffusive transport alone, though the apparent diffusivity is larger than the actual value. The mean species distribution along the channel is thus Gaussian. The variance of this distribution grows linearly in time and is given by

$$\sigma^2 = 2D(1 + \alpha_0 Pe^2)t \tag{14}$$

where the coefficient of dispersion, α_0, is determined by repeated integrals of the velocity profile [36].

$$\alpha_0 = \int_0^1 (u'-1) \int_0^{y^*} \int_0^{y^*} (u'-1)\, dy^* dy^* dy^* = \frac{\delta^2}{30} \tag{15}$$

The term $2Dt$ in Eq. (14) accounts for spreading due to diffusion alone, while the term $2\alpha_0 Pe^2 Dt$ accounts for dispersion.

Substituting Eq. (15) into Eq. (14) and rewriting the result in terms of the dimensionless variables gives the increase in the normalized variance of the species distribution during transport through a turn. The expression obtained, applicable to the region just downstream of the turn, is

$$\left(\frac{\sigma}{a}\right)^2 = \frac{2}{\delta Pe}\left[1 + \frac{(\delta Pe)^2}{30}\right]\theta \tag{16}$$

Neglecting the contribution of streamwise diffusion, this may be written in the simpler form

$$\left(\frac{\sigma}{a}\right)^2 = \frac{1}{15}\,\theta\,\delta Pe \tag{17}$$

By neglecting streamwise diffusion, this latter result describes just that portion of the spreading that is due to dispersion resulting from the turn geometry.

HIGH PECLET NUMBER SOLUTION

Transverse diffusion in the course of a turn cannot significantly redistribute species concentrations across the channel when the Peclet number is large. Each elemental volume of a thin species band instead traverses the turn along a single streamline, and the distance between the leading and trailing edges downstream of the turn is

$$\Delta\ell = U \int_0^\theta \left(\frac{r_o}{u_o} - \frac{r_i}{u_i}\right) d\theta \approx 2\,a\,\theta \tag{18}$$

where u_i and u_o are the local fluid speeds along the inner and outer radii. The left-hand version of this expression is completely general, while the right-hand form applies when the radius of the turn is large compared to the channel width.

More generally, the distance between any two points on the downstream band is $\Delta\ell_{1,2} = 2a\theta(y_2^* - y_1^*)$ when the radius of the turn is large. The downstream distribution is therefore described by a straight line between the two channel walls that is inclined to the direction of motion. The mean species distribution, spatially averaged across the channel width, is thus uniform between the leading and trailing edges, and the variance of such a rectangular distribution is

$$\left(\frac{\sigma}{a}\right)^2 = \frac{1}{12}\left(\frac{\Delta\ell}{a}\right)^2 = \frac{\theta^2}{3} \tag{19}$$

This result is similar to the expression derived by Culbertson in the corresponding limit of a small transit time through the turn [30]. In this previous work, however, the constant 12 above was replaced by an empirical value of about 24 based on a fit to data. This is further discussed later on.

Note that the turn-induced variance at high Peclet numbers is independent of both the turn radius and mean fluid speed. Thus the popular notion that turns of large mean radius reduce dispersion is not correct in this limit. Rather, the spreading in this case depends only on the channel width and included angle of the turn. Note also that the variance is proportional to the square of the included angle in the high Peclet number limit, but varies linearly with the angle when the Peclet number is small.

COMPOSITE SOLUTION

The functional forms of Eqs. (17) and (19) show that the dispersive portion of the variance increases linearly with the Peclet number when the Peclet number is small, but asymptotically approaches a constant when the Peclet number grows large. This suggests that a composite solution of the form

$$\left(\frac{a}{\sigma}\right)^2 = \left(\frac{a}{\sigma}\right)^2_{Pe\to 0} + \left(\frac{a}{\sigma}\right)^2_{Pe\to\infty} \tag{20}$$

might accurately describe the increased variance over all Peclet numbers. Substituting Eqs. (17) and (19) into this expression and rearranging slightly gives

$$\left(\frac{\sigma}{a}\right)^2 = \frac{\theta^2 \delta Pe}{15\,\theta + 3\,\delta Pe} \tag{21}$$

Now adding the contribution to spreading by streamwise diffusion yields

$$\left(\frac{\sigma}{a}\right)^2 = \frac{\theta^2 \delta Pe}{15\,\theta + 3\,\delta Pe} + \frac{2\theta}{\delta Pe} \tag{22}$$

for the total increased variance of the species distribution. This latter result applies just as the species profile emerges from the turn since streamwise diffusion continues to spread the profile in the straight channel segment downstream.

The preceding results were all developed from the perspective of a very thin species band initially entering the turn. However, the variance induced by a turn is always additive with that of the initial distribution, so these results are independent of the width and profile of the band initially entering the turn. The expressions above need only be interpreted as the net increased variance due to the presence of the turn. This additive property, while not immediately obvious, was confirmed using the numerical model described below.

NUMERICAL METHOD

To more generally address distribution broadening induced by turns, we have developed a numerical algorithm for solving the Laplace equation using a novel numerical technique. This technique employs an inverted approach in which the dependent variables are the unknown values of the spatial coordinates and the independent variables are the normalized electric potential, ϕ^*, and an associated stream function, ψ^* [38]. Boundary conditions in the physical domain are readily mapped to the inverted domain using the Cauchy-Riemann compatibility relations. The advantage of this approach is that the computational domain is always rectangular, regardless of the turn geometry, and the curved boundaries of the channel walls appear only as boundary conditions on the rectangular domain. The analysis of transport in complex turn geometries is thus greatly simplified using this method of solution.

The inverted method yields a full two dimensional solution describing the electric potential in the turn and adjoining straight channel segments. Fluid or species velocities are then computed using a normalized form of Eq. (5). This inverted method does not rely on the assumption of a large turn radius, so nonzero radial components of the fluid velocity near the turn entrance and exit are properly described if the geometry of the turn leads to such a condition. This distinguishes the numerical approach from the preceding analysis, where the approximation $\delta \ll 1$ was used in developing Eqs. (9) and (12).

Transient species transport in this numerical scheme is simulated using a Monte Carlo method. Tracer particles are first injected into the straight channel segment several channel widths upstream of the turn. This is followed by a series of steps in which each particle is advected along local lines of constant ψ^*, as it diffuses in both the ϕ^* and ψ^* directions. The length of the advective step is $u^* Pe \Delta t^* S$, based on the local speed, while the length of each diffusive step is $R\sqrt{2\Delta t^*}S$ where R is a normally-distributed random variable having a mean of zero and variance of one [39]; S is the local scale factor relating spatial steps to steps in $\Delta\phi^*$ and $\Delta\psi^*$. All of these steps take place in the orthogonal ϕ^* and ψ^* coordinate system. The advantage of this is that the streamwise diffusion may be neglected in order to more clearly isolate the spreading that results from the turn geometry. Transverse diffusion of course does not contribute to species spreading, but does play an important role in reducing dispersion caused by nonuniform speeds in the turn.

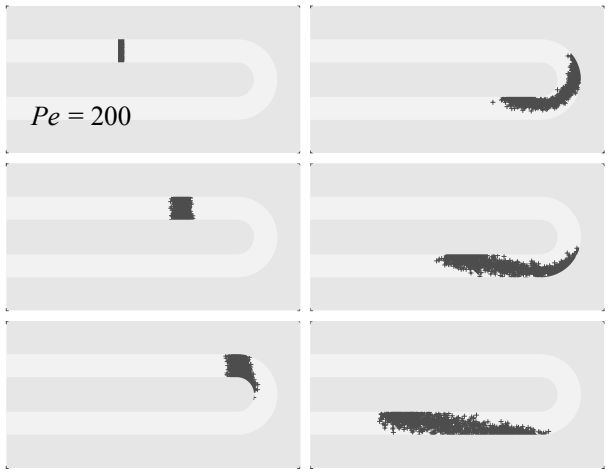

Figure 1. Numerical simulation of the history of species transport through a turn. Band spreading at high Peclet numbers is dominated by skewing induced by the turn geometry. The total turn-induced normalized variance is $(\sigma/a)^2 \approx 3.4$.

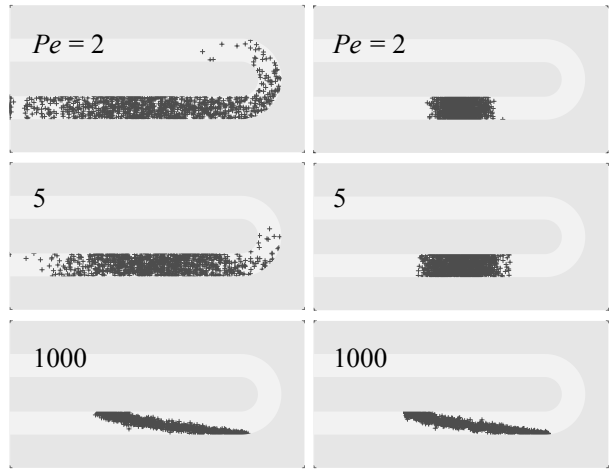

Figure 2. Simulated spreading in a turn. Left column includes streamwise and transverse diffusion; right column neglects streamwise component. Streamwise diffusion increases total spreading, but transverse diffusion reduces dispersive contribution.

Spreading of the species distribution is computed from the final positions of the tracer particles once all of the particles have traversed the turn. The streamwise mean particle position is first computed as the simple average of all positions. The variance of the distribution is then computed as the average sum of the squares of the spatial deviations from the mean. The result is a statistical estimate of σ^2 for the turn. Again either the total variance or that due only to the turn geometry may be computed by respectively including or neglecting the streamwise diffusive steps.

Species spreading due to diffusion in the upstream and downstream straight channel segments must not be included when computing the total variance induced by a turn. This can be managed in one of two ways. The first means is to subtract the quantity $2D(t - \bar{r}\theta/U)$ from the final computed total variance. The second method is to neglect streamwise diffusion during tracer motion whenever a tracer particle resides outside the curved portion of the channel. Both methods yield similar results, though the latter is more accurate when the Peclet number is small and spreading is dominated by diffusion. In this limit, the first method yields the total turn-induced variance as a small difference between two large numbers: the computed total variance for the straight and curved segments, less the estimated spreading by diffusion outside the turn. The second method yields the total variance directly.

Sample results are shown in Fig. 1 for a 180° turn having a inner radius 75% of the channel width. This geometry gives a normalized turn radius of $\bar{r}/a = 1.2$ or, equivalently, $\delta = 0.8$. The series of frames, read from top to bottom along both columns, represents the history of a thin species band traversing the turn at a Peclet number of $Pe = 200$. The time interval between frames is fixed.

The results in Fig. 1 show the normal progression of a species band, including both streamwise and transverse diffusion. Thus the distribution spreads even in the straight channel segment upstream of the turn. As the band approaches the turn, the nonuniform fluid velocity severely skews the distribution profile. Species traveling along the inner radius complete the turn first, followed progressively by species closer to the outer channel wall. The result following the turn is a roughly linear band spanning the channel width but no longer orthogonal to the direction of motion. As this band progresses further along the downstream channel segment, transverse and streamwise diffusion will eventually produce a species distribution that is again uniform across the channel and Gaussian in the direction of motion. The variance of this final distribution once more grows linearly in time.

The spreading illustrated in Fig. 1 results from both dispersion and streamwise diffusion. These two influences can be isolated, somewhat, by including or neglecting streamwise diffusion. Sample calcula-

tions illustrating this are shown in Fig. 2. Here, each frame represents a snapshot of the species distribution downstream of the turn at a fixed time. The turn geometry is the same as that of Fig. 1. The left column in Fig. 2 shows the species distribution resulting from dispersion and both streamwise and transverse diffusion over a range of the Peclet number. Here we see that increasing Peclet numbers generally reduce the width (and variance) of the resulting species distribution.

Frames on the right of Fig. 2 are for the same Peclet numbers as those on the left, but in these only transverse diffusion is included in the calculation. The frames on the right thus represent only that portion of the spreading due to the turn geometry. Here we see that transverse diffusion tends to reduce the spreading that results from the nonuniform velocity field, and the variance of the distribution thus increases with increasing Peclet number.

These general observations are consistent with the analytical results previously discussed. The column on the left of Fig. 2 corresponds to Eq. (22) describing the total variance. As the Peclet number is reduced, the second term on the right of this expression becomes dominant, and the variance of the distribution increases. Equation (21) describes that portion of the variance attributable to the curved geometry and so similarly corresponds to the right-hand column of Fig. 2. This latter expression indicates that the variance generally increases with increasing Peclet number and approaches the asymptotic value $(\sigma/a)^2 = \theta^2/3$ as the Peclet number becomes infinite.

DISCUSSION OF RESULTS

The analysis leading to Eqs. (21) and (22) was based on an assumption that the mean radius of the turn is large compared to the channel width. That is, $\delta = a/\bar{r} \ll 1$. The result for low Peclet numbers, Eq. (17), further employed an assumption that the transit time for traversing the turn was large compared to the characteristic time for diffusion across the channel. This second approximation is equivalent to $t^* = Dt/a^2 = \theta/\delta Pe \gg 1$. Here we examine the applicability of these assumption by comparing the analytical solutions with numerical results. Again, the numerical method relies on no assumptions regarding the turn geometry or transport characteristics. The numerical solutions thus take into account dispersion resulting from nonuniform fluid velocities just upstream and downstream of the turn, as well as radial components of the velocity not described by

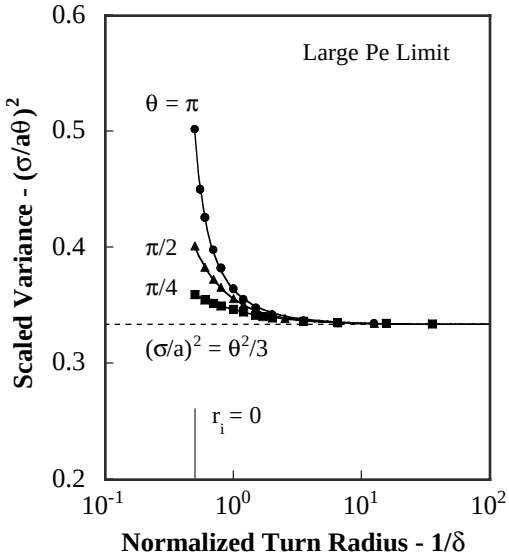

Figure 3. Scaled variance of species distribution computed numerically for large Peclet numbers. The large-radius approximation (dashed curve) remains quite accurate for all turn angles even for $\delta \approx 1$.

Eq. (9). The numerical solutions also account for the true diffusion occurring within the turn, regardless of the value of t^*.

First consider a case for which the Peclet number is infinitely large. In this limit, diffusion plays no role in spreading the species profile, and all spreading results instead from simple skewing of the distribution profile due to the geometry of the turn. By Eq. (19), the variance of the distribution following the turn should be proportional to the square of the included angle. This expression shows no dependence on δ only because the turn radius was assumed to be infinite. To examine the validity of this assumption, we have computed the actual species variance downstream of a turn using the numerical approach. Both streamwise and transverse diffusion are neglected in these calculations, consistent with the case of an infinite Peclet number. The results are shown in Fig. 3 for included angles of 45, 90 and 180 degrees and values of the normalized mean turn radius from 1/2 to 100. Note that the normalized variance here is also scaled by the square of the included angle.

In Fig. 3 we see that the distribution variance induced by a turn is indeed proportional to the square of the included angle and independent of the turn radius when the radius is large compared to the channel width. We also see that the asymptotic value of the variance in this large-radius limit is well approx-

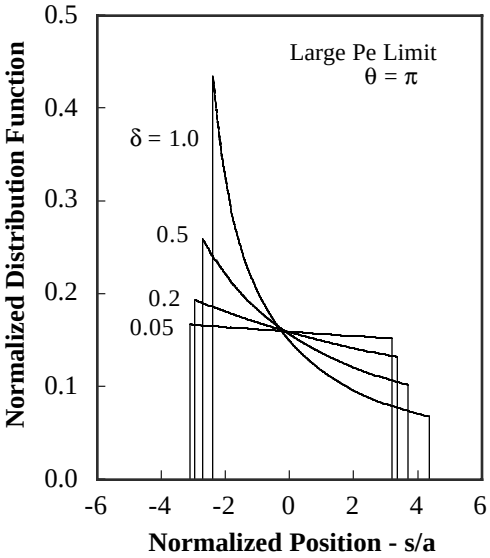

Figure 4. Species distribution downstream of turn. Distribution becomes shifted toward the leading edge as turn radius approaches channel width. Variance of the distribution is nevertheless not much affected.

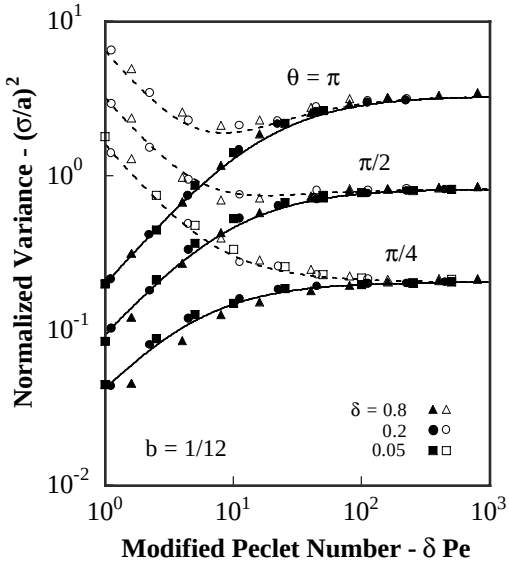

Figure 5. Comparison between analytical (curves) and numerical (symbols) results. Dashed curves and open symbols represent total variance; solid curves and symbols indicate dispersive contribution only.

imated using Eq. (19), as indicated by the dashed curve. Further, this approximation remains valid even when the turn radius is comparable to the channel width. At $\bar{r}/a = 1/\delta = 1$, the computed variance in the high Peclet number limit deviates from $(\sigma/a)^2 = \theta^2/3$ by only about 10, 7 and 4 percent for $\theta = \pi$, $\pi/2$ and $\pi/4$, respectively. The smallest possible normalized turn radius occurs at $r_i = 0$ or $\bar{r}/a = 1/2$, and even here the approximation yields a deviation from the numerical result of only about 50% for $\theta = \pi$.

This broad agreement between the analytical and numerical solutions shown in Fig. 3 suggests that the downstream species distribution remains fairly uniform for all $\delta \geq 1$. That is, the variance of the distribution seems well approximated by $\Delta\ell^2/12$, corresponding to a uniform distribution as expressed in Eq. (19). This is in fact is not the case. The distribution is highly nonuniform except for δ greater than about five.

Figure 4 shows computed species distributions following a 180° turn for several turn radii. The distributions shown are normalized to unit area in the manner of a probability distribution. These species distributions are computed from the tracer particle locations by first constructing the normalized cumulative distribution and then numerically differentiating the cumulative distribution to yield the normalized species distribution. Here we see that the downstream spatial distribution is fairly uniform for $\delta \ll 1$, but is not uniform at all for $\delta \geq 1/2$. For $\delta = 1$, the species concentration between the leading (left) and trailing (right) edges differ by almost a factor of seven. Despite this, the normalized variances of the four distributions shown in Fig. 4 range only from $(\sigma/a)^2 = 3.60$ for $\delta = 1$ to 3.29 for $\delta = 0.05$. Thus the wide range of applicability of Eq. (19) appears to be mainly a happy coincidence based on offsetting second-order contributions to the turn-induced variance; it does not indicate that the downstream species distribution is uniform.

Figure 5 shows a more general comparison between the variance computed analytically using Eqs. (21) and (22) and values computed by numerical means. In this case the normalized variance is plotted as a function of the modified Peclet number, δPe. By Eqs. (21) and (22), the computed variance should depend only on the included angle and this parameter. As such, the numerically-computed total variance and the dispersive contribution should each fall on a single curve identified only by the included angle, regardless of the turn radius. We see that this is indeed generally the case. The analytical and numerical solutions describing both the total and dispersive variance are in very good agreement over most of the conditions shown, confirming the

validity of the analytical results. These conditions span $\pi/4 \leq \theta \leq \pi$ and $0.05 \leq \delta \leq 0.8$ and thus represent nearly the entire range of turn geometries of practical interest.

Each symbol in Fig. 5 represents the variance computed numerically for the specified conditions using 1000 tracer particles, thus the expected accuracy of these statistical estimates is thus about $\pm 3\%$. The height of the symbols represent a variation of about 10%, so any symbol touching its corresponding curve indicates that the deviation between analytical and numerical results is at most 8%.

The most significant deviations between the analytical and numerical solutions occurs when δ is large but both δPe and the included angle are small. This is most apparent in the triangles at the left of the two lower curves for $\theta = \pi/2$ and $\pi/4$; triangles correspond to $\delta = 0.8$. That the analytical solutions lose accuracy when δ is large is not surprising since the analysis was based on an assumption that $\delta \ll 1$. It is surprising, however, that the loss of accuracy is greatest when the included angle is small. For $\theta = \pi$, the analytical solution still appears to be very good at similar δPe even for $\delta = 0.8$. Likewise, this behavior cannot be explained simply by a breakdown of the low Peclet number assumption that $t^* = \theta/\delta Pe$ is large. The value of t^* along each curve is a function of δPe only, so this also cannot account for the loss of accuracy for non-negligible δ when the included angle is small. This behavior remains something of a mystery and likely results from a growing imbalance in offsetting errors generated by both of these assumptions.

OPTIMUM TURN GEOMETRY

The results in Fig. 5 indicate that increased variance of the species distribution downstream of a turn always decreases with decreasing Peclet number in the absence of streamwise diffusion. The variance of the distribution attributable to the turn geometry is thus minimized by minimizing the Peclet number, as illustrated in the right-hand columns of Fig. 2. However, low Peclet numbers lead to significant spreading due to streamwise diffusion, and because of this the total variance, expressed by Eq. (22), exhibits a minimum at the condition

$$\delta Pe = \frac{30\,\theta}{\sqrt{30}\,\theta - 6} \tag{23}$$

This result defines either an optimum geometry for a given Peclet number and included turn angle or an optimum Peclet number for a given turn geometry. Note that this optimum condition exists only for included angles $\theta > \sqrt{6/5}$ or $\theta > 63°$. For smaller angles the turn-induced dispersion is too small to provide the tradeoff between dispersion and streamwise diffusion needed to yield a minimum.

Although the equation above defines an optimum condition for minimum total spreading, the benefit of this optimum is fairly small. Substituting Eq. (23) into Eq. (22) yields

$$\left(\frac{\sigma}{a}\right)^2 = \frac{4\theta}{\sqrt{30}} - \frac{2}{5} \tag{24}$$

For $\theta = \pi$, this gives $(\sigma/a)^2 \approx 1.89$. In comparison, the maximum variance in the high Peclet number limit is only $(\sigma/a)^2 = \theta^2/3 \approx 3.29$. Thus the minimum dispersion for this turn is still nearly 60% of the high Peclet number value.

One useful means of interpreting the normalized variance $(\sigma/a)^2$ is to compute the length of a straight channel segment, L, yielding the same increased variance by diffusion alone. The variance for the diffusion problem is $\sigma^2 = 2Dt$, where $t = L/U$. Combining these expressions and normalizing the length by the channel width gives

$$L^* = \frac{L}{a} = \frac{Pe}{2}\left(\frac{\sigma}{a}\right)^2 \tag{25}$$

Based on the minimum above of $(\sigma/a)^2 \approx 1.89$, this yields $L^* = 189$ at a Peclet number of only 200. Such a turn would thus increase the distribution variance by the same amount as a straight channel segment of a length equal to about 200 channel widths. For a Peclet number of 1000, this length would increase to nearly 1000 channel widths.

COMPARISON WITH PRIOR STUDY

Culbertson et al. [30] previously investigated the geometric dispersion induced by microchannel turns. They developed an analytical model based on a high Peclet number solution like that derived here, but employed an empirical relation to describe the distribution variance when the Peclet number is small. The form of their expression is

$$\left(\frac{\sigma}{a}\right)^2 = \frac{4\theta^2}{X}\left(1 - e^{-At_d/t_t}\right)^2 \tag{26}$$

where $X = 23.7$ and $A = 0.977$ were obtained from a least-squares fit to measured results over a wide range of conditions spanning $0.08 \leq \delta \leq 0.48$ and $10 \leq Pe \leq 420$.

This correlation and Eq. (21) are similar in the limit of a high Peclet number, except for the constant $X \approx 24$ in Eq. (26). This constant corresponds exactly to the 12 appearing in Eq. (19). In this limit, Eq. (26) thus yields a normalized variance of about one-half that given by Eq. (21).

At lower Peclet numbers, the Culbertson correlation accounts for the influence of transverse diffusion through a dimensionless ratio of the characteristic time for diffusion across the channel width to the time for transit through the turn. They defined this ratio as

$$\frac{t_d}{t_t} = \frac{a^2 U \bar{r}}{2D\theta(\bar{r} + a/2)^2} = \frac{\delta Pe}{2\theta(1+\delta/2)^2} \qquad (27)$$

This ratio is nearly the inverse of t^* given in Eq. (13), but contains some additional dependence on the turn geometry as expressed by the term $2(1+\delta/2)^2$. This ratio further contains the Peclet number only in the product δPe, which is consistent with our present analytical solution. However, the behaviors of Eq. (21) and Eq. (26) are quite different when the Peclet number is small. Expanding Eq. (26) for $t_d/t_t \to 0$ gives

$$\left(\frac{\sigma}{a}\right)^2 \sim \frac{A^2}{X}\frac{(\delta Pe)^2}{(1+\delta/2)^4} \quad \text{as} \quad Pe \to 0 \qquad (28)$$

Equation (26) thus yields a normalized variance that is proportional to the square of δPe and independent of the included angle when the Peclet number is small. In contrast, Eq. (21) indicates that the variance should be proportional to $\theta\delta Pe$ in this limit.

These differences between Eqs. (21) and (26) are illustrated in Fig. 6. Here both are plotted as a function of the Peclet number for a range of values of δ. It is clear from this that the turn-induced variance expressed by Eq. (26) is always significantly lower than the values given by Eq. (21), and this disparity grows larger as the Peclet number falls.

The apparent explanation for these large discrepancies is that the channels used by Culbertson had tapered sidewalls, and the widths they reported were the widths at the channel top. Their channels were produced by an isotropic etch of soda-lime glass, so the mean channel width was always smaller than the width at the top. Their reported values of the normalized variance, scaled by the top channel width, are thus smaller than the values obtained by scaling the same raw data using the mean width instead. If Culbertson et al. had normalized the variance using the mean channel width, we expect that their fit would have yielded $X \approx 12$ in keeping with

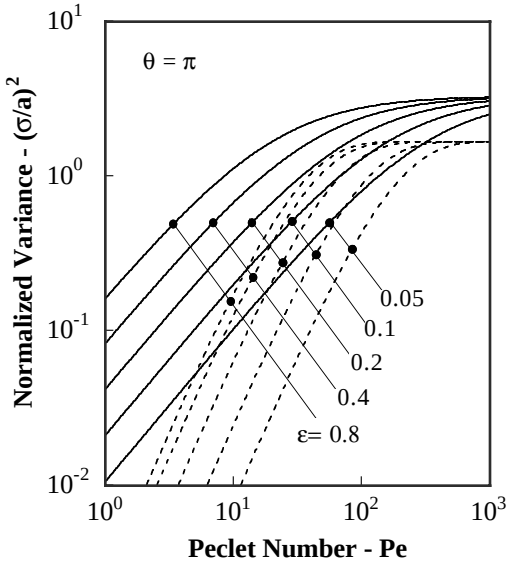

Figure 6. Comparison between Eqs. (21) and (26). Previous expression (dashed curves) yields a normalized variance much smaller than present solution (solid) for all Peclet numbers and turn radii.

Eq. (19) of the present study. Since the variance in the high Peclet number limit is proportional to the square of the channel width, even small discrepancies between the top and mean widths can have a significant influence.

To illustrate the effect of tapered sidewalls, we have computed the turn-induced variance using Eq. (21) for the range of parameters appearing in Culbertson's paper. The results are plotted in Fig. 7, along with Culbertson's data, using the axes t_d/t_t and $(\sigma/2\theta w)^2$ to replicate Fig. 4 of their paper. Here w is the top channel width.

Two sets of curves are shown in Fig. 7. The upper set represent the result from Eq. (21) using $a = w$. Values along the lower set of curves are also computed from Eq. (21), but in this case the channel width is taken as $a = w - h$, where h is the channel depth. This expression yields the mean channel width for a 45° sidewall angle. Actual channel depths were not reported by Culbertson; here we use $h = 10$ μm as the presumed depth based on values for similar channel widths reported elsewhere by these authors [7].

Each curve set in Fig. 7 consists of nine curves corresponding to all permutations of $\bar{r} = 125, 250$ and 500 μm with $w = 38, 47$ and 60 μm of the Culbertson study. A single curve thus represents one value of the normalized turn radius, $\bar{r}/a = 1/\delta$. For each value

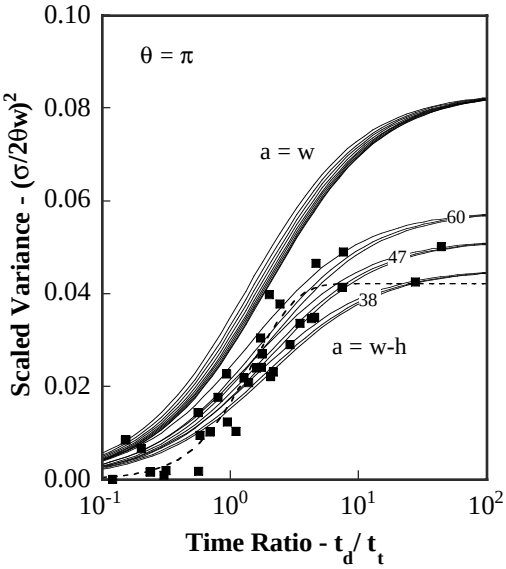

Figure 7. Comparison between present analysis and data of Culbertson et al. Equation (21) is in good agreement with measured results when evaluated using the mean channel width, $a = w - h$.

of δ, Eq. (27) is used to compute δPe from t_d/t_t, and the variance is then computed using Eq. (21). These appear as a separate curves here because t_d/t_t is not quite equivalent to δPe appearing in Eq. (21).

Note that the curves of the lower set segregate into three groups for large t_d/t_t. These three groups correspond to the three channel widths, as indicated by the numerals toward the right of the plot. The reason for this segregation is that the relative influence of sidewall taper on the mean channel width depends on the top channel width. For a fixed channel depth and sidewall angle, the top channel width is relatively close to the mean width when the channel is wide compared to the depth. In this case, the condition $a \approx w$ is approached. As the channel becomes smaller, the top and mean widths diverge, approaching a minimum of $a \approx w/2$, and the scaled variance $(\sigma/2\theta w)^2$ based on the top width decreases. This is of course just an artifact of scaling since the actual variance is simply proportional to the square of the mean channel width.

The dashed curve in Fig. 7 represents Eq. (26) developed by Culbertson. The constants in this expression were obtained by fitting the data shown. While Eq. (26) captures the general trend of the data, there appears to remain significant scatter about this fit. In contrast, the results of our present analysis bound most of this apparent scatter, suggesting that the deviations from Eq. (26) may in fact have some physical basis. The original data reported by Culbertson were identified by the mean turn radius, but not by the channel width. Thus it is not possible to associate specific data points with specific curves as both values are needed to compute δ. Still, Eq. (21) appears likely to provide a better fit to the data than does Eq. (26).

Tapered channel walls appear to resolve the major differences between Eqs. (21) and (26). These two expressions are not equivalent, however, in either the low or high Peclet number limits. Equation (26) is specific to the channels used in the Culbertson study since the constant $X = 23.7$ seems to carry a hidden dependence on the channel width, depth and sidewall angle. In contrast, Eq. (21) is universal and is applicable to either vertical or tapered sidewalls, provided that the channel width, a, is taken as the mean width over the depth of the channel.

SUMMARY

Here we examine the spreading of a species band induced by electrophoretic or electroosmotic transport through a two-dimensional turn. Analytical solutions to the governing transport equations are obtained in the limits of low and high Peclet numbers. From these asymptotic behaviors, we construct a composite solution applicable to all Peclet numbers. Numerical solutions are also presented for a variety of turn geometries and a wide range of the Peclet number. These solutions rely on no approximations regarding either the Peclet number or geometry of the turn.

We find that the band spreading due to transport through by a turn is well described for all Peclet numbers by the composite solution

$$\left(\frac{\sigma}{a}\right)^2 = \frac{\theta^2 \delta Pe}{15\,\theta + 3\,\delta Pe} + \frac{2\theta}{\delta Pe}$$

where σ^2 is the total increased variance of the downstream species distribution, a is the mean channel width, θ is the included angle of the turn, δ is the ratio of the channel width to the mean turn radius, and $Pe = Ua/D$ is the Peclet number based on the mean channel width and fluid or species speed. The first term on the right of this expression describes the dispersive contribution to the total variance; the second term describes the additional contribution of streamwise diffusion.

This analytical expression is based on an assumption that the radius of the turn is much larger

than the channel width. Despite this assumption, the expression provides accurate results even when the turn radius is comparable to the channel width. Based on comparisons with our numerical results, we find that it yields both the dispersive component and total variance to within about 10% for all Peclet numbers, all $\bar{r}/a = 1/\delta \geq 1$, and included turn angles up to 180°.

The dispersive portion of the turn-induced variance in the high Peclet number limit is proportional to the squares of the channel width and the included turn angle, but is independent of both the Peclet number and radius of the turn. As such, more gradual turns do not reduce the variance when the product δPe is larger than about five times the included angle. On the contrary, large radius turns generally increase the total variance owing to the added contribution of streamwise diffusion. At low Peclet numbers, we find that the dispersive portion of the total variance is proportional to the product $\theta\delta Pe$. In this limit, the dispersive variance is thus inversely proportional to the turn radius. In contrast, the total variance grows in proportion to the turn radius when the Peclet number is small.

Based on the expression above, the total turn-induced variance exhibits a minimum between the extremes of low and high Peclet number if the included angle of the turn is greater than about 63°. The optimum condition defines either a preferred Peclet number for a fixed turn geometry or a preferred geometry for a fixed Peclet number. The total variance at this minimum is about a factor of two below the value in the high Peclet number limit for a 180° included angle. While this is a significant reduction, it may not provide any real practical benefit when the Peclet number is large. When the Peclet number is small, however, a large turn radius should be avoided to limit band spreading by diffusion. In this case, the benefit of the optimum geometry can be very large since diffusive spreading may far exceed that due to the turn geometry when the Peclet number is small.

Finally, this analytical expression is compared with experimental results previously obtained by Culbertson et al. We find that the dispersive portion of the expression agrees well with their data, provided that the mean channel width properly accounts for the channel sidewall taper.

NOMENCLATURE

a	mean channel width
c	species concentration
c_e	ion concentration
D	binary diffusivity
E	applied electric field
F	Faraday constant
L	distance of travel: $L = Ut$
Pe	Peclet number: $Pe = Ua/D$
s	streamwise position
r	radial position
$\bar{r}$	mean turn radius: $\bar{r} = (r_i + r_0)/2$
t	time
u	streamwise fluid speed
$\mathbf{u}$	local fluid velocity
U	mean fluid speed
w	top channel width
y	transverse position
z	charge number
ϵ	dielectric constant
ζ	surface electric potential
θ	angular position or included angle of turn
λ	Debye length
μ	viscosity
ρ_e	charge density
σ^2	increased variance of species distribution
ϕ	electric potential
ω	angular speed: $\omega = U/\bar{r}$

Normalized Variables

$\mathbf{E}$	electric field: $\mathbf{E} = -\nabla\phi/E_x$
r^*	radial position: $r^* = r/\bar{r}$
s^*	streamwise position: $s^* = (\theta - \omega t)\bar{r}/a$
t^*	time: $t^* = Dt/a^2$
u^*	local fluid speed: $u^* = u/U$
y^*	transverse position: $y^* = y/a$
λ^*	Debye length: $\lambda^* = \lambda/a$
ζ^*	surface potential: $\zeta^* = zF\zeta/RT$

Subscripts and Superscripts

i, o	on inner or outer radius

ACKNOWLEDGMENT

This work was funded by a Sandia Phenomenological Modeling and Engineering Simulations LDRD. Sandia National Laboratories is operated by Sandia Corporation for the United States Department of Energy under contract DE-AC04-94AL85000.

REFERENCES

1. A. Manz, J. C. Fettinger, E. Verpoorte, H. Ludi, H. M. Widmer and D. J. Harrison, "Micromachining of Monocrystalline Silicon and Glass for chemi-

cal Analysis Systems," *Trends Anal. Chem.*, **10**, 144-149, 1991.
2. A. Manz, D. J. Harrison, E. M. J. Verpoorte, J. C. Fettinger, A. Paulus, H. Ludi and H. M. Widmer, "Planar Chips Technology for Miniaturization and Integration of Separation Techniques into Monitoring Systems: Capillary Electrophoresis on a Chip," *J. Chromatogr.*, **593**, 253-258, 1992.
3. D. J. Harrison, A. Manz, Z. H. Fan, H. Ludi and H. M. Widmer, "Capillary Electrophoresis and Sample Injection Integrated on a Planar Glass Substrate," *Anal. Chem.*, **64**, 1926-1932, 1992.
4. C. Effenhauser, A. Manz and H. M. Widmer, "Glass Chips for High Speed Capillary Electrophoresis Separations with Submicrometer Plate Heights," *Anal. Chem.*, **65**, 2637-2642, 1993.
5. S. C. Jacobson, R. Hergenroder, L. B. Koutny and J. M. Ramsey, "High-Speed Separations on a Microchip," *Anal. Chem.*, **66**, 1114-1118, 1994.
6. S. C. Jacobson, C. T. Culbertson, J. E. Daler and J. M. Ramsey, "Microchip Structures for Submillisecond Electrophoresis," *Anal. Chem.*, **70**, 3476-3480, 1998.
7. S. C. Jacobson and J. M. Ramsey, "Integrated Microdevice for DNA Restriction Fragment Analysis," *Anal. Chem.*, **68**, 720-723, 1996.
8. N. Chiem and D. J. Harrison, "Microchip-Based Capillary Electrophoresis for Immunoassays: Analysis of Monoclonal Antibodies and Theophylline," *Anal. Chem.*, **69**, 373-378, 1997.
9. R. M. McCormick, R. J. Nelson, M. G. Alonson-Amigo, D. J. Benvegnu and H. H. Hooper, "Microchannel Electrophoretic Separations of DNA in Injection-Molded Plastic Substrates," *Anal. Chem.*, **69**, 2626-2630, 1997.
10. C. S. Effenhauser, G. J. M. Bruin, A. Paulus and M. Ehrat, "Integrated Capillary Electrophoresis on Flexible Silicone Microdevices: Analysis of DNA Restriction Fragments and Detection of Single DNA Molecules on Microchips," *Anal. Chem.*, **69**, 3451-3457, 1997.
11. L. C. Waters, S. C. Jacobson, N. Kroutchinina, J. Khandurine, R. S. Foote and J. M. Ramsey, "Multiple Sample PCR Amplification and Electrophoretic Analysis on a Microchip," *Anal. Chem.*, **70**, 5172-5176, 1998.
12. F. Von Heeren, E. Verpoorte, A. Manz and W. Thormann, "Micellar Electrokinetic Chromatography Separations and Analysis of Biological Samples on a Cyclic Planar Microstructure," *Anal. Chem.*, **68**, 2044-2053, 1996.
13. M. A. Northrup, B. Benett, D. Hadley, P. Landre, S. Lehew, J. Richards and P. Stratton, "A Miniature Analytical Instrument for Nucleic Acids based on Micromachined Silicon Reaction Chambers," *Anal. Chem.*, **70**, 918-922, 1998.
14. A. T. Woolley, G. F. Sensabaugh and R. A. Mathies, "High-Speed DNA Genotyping Using Microfabricated Capillary Array Electrophoresis Chips," *Anal. Chem.*, **69**, 2181-2186, 1997.
15. S. C. Jacobson, R. Hergenroder, A. W. Moore, Jr., and J. M. Ramsey, "Precolumn Reactions with Electrophoretic Analysis Integrated on a Microchip," *Anal. Chem.*, **66**, 4127-4132, 1994.
16. S. C. Jacobson, L. B. Koutny, R. Hergenroder, A. W. Moore, Jr., and J. M. Ramsey, "Microchip Capillary Electrophoresis with Integrated Postcolumn Reactor," *Anal. Chem.*, **66**, 3472-3476, 1994.
17. H. Salimi-Moosavi, T, Tang and D. J. Harrison, "Electroosmotic Pumping of Organic Solvents and Reagents in Microfabricated Reactor Chips," *J. Am. Chem Soc.*, **119**, 8716-8717, 1997.
18. P. K. Dasgupta and S. Liu, "Auxiliary Electroosmotic Pumping in Capillary Electrophoresis," *Anal. Chem.*, **66**, 3060-3065, 1994.
19. H. Salimi-Moosavi, T, Tang and D. J. Harrison, "Electrokinetic Control of Fluid Flow in Native Poly(Dimethylsiloxane) Capillary Electrophoresis," *Electrophoresis*, **21**, 107, 2000.
20. S. C. Jacobson, R. Hergenroder, L. B. Koutny and J. M. Ramsey, "Open Channel Electrochromatography on a Microchip," *Anal. Chem.*, **66**, 2369-2373, 1994.
21. C. Yan, R. Dadoo, H. Zhao, R. N. Zare and D. J. Rakestraw, "Capillary Electrochromatography: Analysis of Polycyclic Aromatic Hydrocarbons," *Anal. Chem.*, **67**, 2026-2029, 1995.
22. C. Ericson, J. Holm, T. Ericson and S. Hjerten, "Electroosmosis- and Pressure-Driven Chromatography in Chips Using Continuous Beds," *Anal. Chem.*, **72**, 81-87, 2000.
23. J. P. Kutter, S. J. Jacobson and J. M. Ramsey, "Integrated Microchip Device with Electrokinetically Controlled Solvent Mixing for Isocratic and Gradient Elution in Micellar Electrokinetic Chromatography," *Anal. Chem.*, **69**, 5165-5171, 1997.
24. J. P. Kutter, S. J. Jacobson, N. Matsubara and J. M. Ramsey, "Solvent-programmed Microchip Open-Channel Electrochromatography," *Anal. Chem.*, **70**, 3291-3297, 1998.
25. J. P. McEldoon and B. Datta, "Analytical Solution for Dispersion in Capillary Chromatography with Electroosmotic Flow," *Anal. Chem.*, **64**, 227-230, 1992.
26. M. Martin and G. Guiochon, "Axial Dispersion in Open-Tubular Capillary Liquid Chromatography

with Electroosmotic Flow, *Anal. Chem.*, **56**, 614-620, 1984.
27. S. K. Griffiths and R. H. Nilson, "Hydrodynamic Dispersion of a Neutral Non-Reacting Solute in Electroosmotic Flow," *Anal. Chem.*, **71**, 5522-5529, 1999.
28. J. C. Giddings, "Coiled Columns and Resolution in Gas Chromatgraphy," *J. Chromatog.*, **3**, 520-523, 1960.
29. V. Kasicka, Z. Prusik, B. Gas and M. Stedry, "Contribution of Capillary Coiling to Zone Dispersion in Capillary Zone Electrophoresis," *Electrophoresis*, **16**, 2034-2038, 1995.
30. C. T. Culbertson, S. C. Jacobson and J. M. Ramsey, "Dispersion Sources for Compact Geometries on Microchips," *Anal. Chem.*, **70**, 3781-3789, 1998.
31. E. B. Cummings, S. K. Griffiths, R. H. Nilson and P. H. Paul, "Conditions for Similitude Between the Electric Field and Fluid Velocity in Electroosmotic Flow," Sandia National Laboratories Report, SAND99-8246, 1999. Accepted for publication in *Analytical Chemistry.*
32. H. P. G. Darcy, *Les Fontaines Publiques de la Ville de Dijon*, Dalmont, Paris, 1856.
33. P. G. Saffman, "Viscous Fingering in Hele-Shaw Cells," *J. Fluid. Mech*, **173**, 73-94, 1986.
34. G. I. Tayor, "Dispersion of Soluble Matter in Solvent Flowing Slowly Through a Pipe," *Proc. Roy. Soc. Lond.*, **A 219**, 186-203, 1953.
35. G. I. Taylor, "Conditions Under Which Dispersion of a Solute in a Stream Can be Used to Measure Molecular Diffusion," *Proc. Roy. Soc. Lond.*, **A 225**, 473-477, 1954.
36. R. Aris, "On the Dispersion of a Solute in Fluid Flowing Through a Tube," *Proc. Roy. Soc. Lond.*, **A 235**, 67-77, 1956.
37. P. C. Chatwin, "The Approach to Normality of the Concentration Distribution of a Solute in a Solvent Flowing Along a Straight Pipe," *J. Fluid Mech.*, **43**, 321-352, 1970.
38. R. W. Jeppson, "Numerical Solutions to Free-Surface Axisymmetric Flows," *J. Eng. Mech. Div. Am. Soc. Civ. Eng.*, **95**, 1, 1969.
39. A. L. Fogelson, "Particle Method Solution of Two-Dimensional Convection-Diffusion Equations," *J. Comp. Phys.*, **100**, 1-16, 1992.

DISTRIBUTION

1	MS 0149	C. E. Meyers, 4000
1	MS 0710	A. P. Sylwester, 6245
1	MS 0826	W. L. Hermina, 9111
1	MS 0826	D. R. Noble, 9111
1	MS 0826	P. R. Schunk, 9111
1	MS 0827	C. C. Wong, 9114
1	MS 0843	A. C. Ratzel, 9112
1	MS 1413	T. E. Michalske, 1115
1	MS 1425	D. R. Adkins, 1715
1	MS 1425	G. C. Frye-Mason, 1715
1	MS 9001	M. E. John, 8000
		Attn: R. C. Wayne, 2200
		D. R. Henson, 8400
		P. N. Smith, 8500
		K. E. Washington, 8900
10	MS 9042	S. K. Griffiths, 8728
10	MS 9042	R. H. Nilson, 8728
1	MS 9042	M. W. Perra, 8728
1	MS 9051	R. S. Larson, 8728
1	MS 9051	P. H. Paul, 8355
1	MS 9054	W. J. McLean, 8300
		Attn: D. R. Hardesty, 8361
		F. P. Tully, 8353
		R. W. Carling, 8362
1	MS 9056	J. Vitko, 8100
1	MS 9056	D. L. Lindner, 8102
1	MS 9161	W. Bauer, 8358
1	MS 9214	C. F. Melius, 8130
1	MS 9401	J. M. Hruby, 8702
1	MS 9405	T. M. Dyer, 8700
		Attn: R. Q. Hwang, 8721
		K. L. Wilson, 8722
		J. C. F. Wang, 8723
		G. J. Thomas, 8724
		W. A. Kawahara, 8725
		E. P. Chen, 8726
		J. L. Handrock, 8727
1	MS 9671	D. W. Arnold, 8358
1	MS 9671	C. G. Bailey, 8358
1	MS 9671	E. B. Cummings, 8355
1	MS 9671	E. F. Hasselbrink, 8355
1	MS 9671	D. J. Rakestraw, 8358
1	MS 9671	J. S. Schoeniger, 8120
3	MS 9018	Central Technical Files, 8940-2
4	MS 0899	Technical Library, 4916
1	MS 9021	Technical Communications Dept., 8815/ Technical Library, MS 0899, 4916
2	MS 9021	Technical Communications Dept., 8815 for DOE/OSTI